were refined anisotropically. The positions of hydrogen atoms were calculated (C-H = 0.95 Å) and were included as fixed contributions to the structure factors. Each hydrogen atom was assigned an isotropic thermal parameter 1.2 times that of the atom to which it is attached. No solvent hydrogen atoms were included. The final cycle of refinement on F, involving 1578 observations and 238 variables, converged to the agreement indices given in Table I. The final difference electron density map revealed residual electron density (0.19-0.22 e/Å^3) in the vicinity of the solvate molecule. Crystallographic details are summarized in Table I. The positional parameters and equivalent isotropic thermal parameters for non-hydrogen atoms are listed in Table II. Selected bond distances and angles are presented in Table III.

Acknowledgment. We thank the U.S. NIH, the U.S. DOE., the Pohang Institute of Science and Technology, and the Korea Science and Engineering Foundation for support. We also gratefully acknowledge Professor J. A. Ibers of Northwestern University for obtaining high-resolution mass spectra and Dr. S. R. Wilson and Mr. D. Whang for assistance with the X-ray crystallographic data. G.S.G. and K.S.S. are recipients of A. P. Sloan Research Fellowships, G.S.G. acknowledges a Henry and Camille Dreyfus Teacher-Scholar Award, and K.S.S. an NIH Research Career Development Award.

Supplementary Material Available: Tables of anisotropic thermal parameters, complete bond distances and angles, least-squares planes, and dihedral angles (6 pages); a listing of observed and calculated structure factors (8 pages). Ordering information is given on any current masthead page.

Contribution from the Department of Chemistry,
New York University, New York, New York 10003

Models of Amide-Cysteine Hydrogen Bonding in Rubredoxin: Hydrogen Bonding between Amide and Benzenethiolate in $[(CH_3)_3NCH_2CONH_2]_2[Co(SC_6H_5)_4]\cdot{}^1/_2CH_3CN$ and $[(CH_3)_3NCH_2CONH_2][SC_6H_5]$†

Marc Anton Walters,* John C. Dewan, Caroline Min, and Shirley Pinto

Received January 8, 1991

Amide-thiolate hydrogen-bonding interactions are described for the cobalt complex $[(CH_3)_3NCH_2CONH_2]_2[Co(SC_6H_5)_4]\cdot{}^1/_2CH_3CN$ (**1**) and the metal-free salt $[(CH_3)_3NCH_2CONH_2][SC_6H_5]$ (**2**). Complex **1** has a triclinic cell with space group $P\bar{1}$, a = 16.960 (5) Å, b = 17.874 (6) Å, c = 14.184 (6) Å, α = 111.47 (3)°, β = 94.34 (3)°, γ = 70.50 (2)°, and Z = 4. Complex **2** has a monoclinic cell with space group $P2_1/n$, a = 12.847 (9) Å, b = 6.730 (5) Å, c = 29.268 (4) Å, β = 95.65 (2)°, and Z = 8. Compound **1** serves to model amide-cysteine hydrogen bonding and its effect on metal coordination in rubredoxin. Average N-H···S hydrogen bond lengths are 3.356 (7) and 3.306 (3) Å for **1** and **2**, respectively. In **1** the average Co-S_N bond length (S_N = non-hydrogen-bonding sulfur) is 2.294 (2) Å, shorter by 0.034 Å than the average Co-S bond length of 2.328 (4) Å in the complex $[(C_6H_5)_4P]_2[Co(SC_6H_5)_4]$, in which hydrogen bonding is absent. The average Co-S_H bond length (S_H = hydrogen-bonded sulfur) in **1** is 2.320 (2) Å, equivalent to that in $[(C_6H_5)_4P]_2[Co(SC_6H_5)_4]$. More generally the average Co-$S_{(N+H)}$ bond length in **1**, 2.302 (1) Å, is 0.026 Å shorter than that of the non-hydrogen-bonding complex. These results suggest that a local stabilization of the $[Co(SC_6H_5)_4]^{2-}$ complex results from hydrogen bonding. Vibrational bands assigned to metal-ligand modes of approximate T_2 and A_1 symmetry are observed at 237, 231, 218, and 204 cm^{-1}, respectively, for **1** as compared with 235, 228, 220, and 201 cm^{-1} in $[(CH_3)_4N]_2[Co(SC_6H_5)_4]$, a non-hydrogen-bonding complex. The direction of the metal-ligand vibrational frequency shifts with hydrogen bonding is in agreement with X-ray crystallographic data. These results suggest that amide-cysteine hydrogen bonding may stabilize the iron-containing redox center in rubredoxin and thereby account for its relatively high redox potential.

Introduction

Hydrogen bonding between amide groups and cysteine sulfur is a feature of all iron-sulfur proteins.[1] Much of the importance of the N-H···S interaction derives from the fact that it may modulate the redox potentials of several of these proteins.[1,2] In rubredoxin (Rd), the $Fe^{2+/3+}$ redox couple occurs in the vicinity of -0.05 V, as determined by reduction in the presence of NADPH and NADPH-ferredoxin reductase.[3,4] Synthetic iron tetrathiolate complexes by contrast have redox potentials in the vicinity of -1.0 V versus SCE in organic media.[4,5-7] The most important factors that may account for differences in protein and model complex redox potentials are the high solvent dipole moment of water and amide-cysteine (N-H···S) hydrogen bonding in the protein. Positive redox potential shifts have been observed for iron(II) tetrathiolate complexes in micelles in aqueous solution,[2,8] which supports the idea of a solvent dipole moment influence. The redox couple of the $[Fe(S_2\text{-}o\text{-}xyl)_2]^{-/2-}$ complex shifts from -0.99 V versus SCE in Me_2SO to -0.64 V in aqueous micelles. In the same environment the peptide complex[8] [Fe(*Z*-Cys-Pro-Leu-Cys-OMe)$_2$]$^{2-}$ exhibits a redox potential of -0.37 V versus SCE, very close to the potential observed in native Rd.[4] It has been suggested that this effect is, in part, due to favorable N-H···S hydrogen bonding to sulfur in a peptide sequence identical with that at the metal binding site of the protein.[8] In principle hydrogen bonding would decrease the crystal field at the metal center to a greater extent for the reduced rather than for the oxidized complex.

There has been a need for information in the study of hydrogen bonding in synthetic analogues of Rd. The present work addresses

† This work was presented in preliminary form at the 199th National Meeting of the American Chemical Society, April 22-27, 1990, Boston, MA.

(1) Adman, E. T. *Biochim. Biophys. Acta* **1979**, *549*, 107-144.
(2) Nakamura, A.; Ueyama, N. In *Metal Clusters in Proteins*; Que, L., Ed.; American Chemical Society: Washington, DC, 1988; Chapter 14.
(3) Lovenberg, W.; Sobel, B. E. *Proc. Natl. Acad. Sci. U.S.A.* **1965**, *54*, 193-199.
(4) Peterson, J. A.; Coon, M. J. *J. Biol. Chem.* **1968**, *243*, 339-334.
(5) Lane, R. W.; Ibers, J. A.; Frankel, R. B.; Holm, R. H. *Proc. Natl. Acad. Sci. U.S.A.* **1975**, *72*, 2866-2872.
(6) Lane, R. W.; Ibers, J. A.; Frankel, R. B.; Papaefthymiou, G. C.; Holm, R. H. *J. Am. Chem. Soc.* **1977**, *99*, 84-98.
(7) Moura, I.; Moura, J. J. G.; Santos, M. H.; Xavier, A. V.; LeGall, J. *FEBS Lett.* **1979**, *107*, 419-421.
(8) Nakata, M.; Ueyama, N.; Fuji, M.-A.; Nakamura, A.; Wada, K.; Matsubara, H. *Biochim. Biophys. Acta* **1984**, *788*, 306-312.

0020-1669/91/1330-2656$02.50/0

this problem with an examination of an anionic metal chalcogenide complex acting as an acceptor to an amide hydrogen-bond donor. In using X-ray crystallography to characterize these analogues, we can infer the effect of hydrogen bonding on the stability and redox potential of the complex. Results show a sizable decrease in certain Co–S bond lengths with direct structural evidence for electron delocalization involving the orbitals of the amide hydrogen-bond acceptor. These effects are measurable by vibrational spectroscopy and are consistent with the net stabilization of the ground state of the metal complex. Hydrogen bonding may act in a similar fashion in iron–sulfur proteins, which are rich in amide–cysteine hydrogen bonds at the metal binding site.

Experimental Section

Synthesis of $[(CH_3)_3NCH_2CONH_2]Cl$. (Carbamoylmethyl)trimethylammonium chloride ((CTA)Cl) was synthesized by a modification of the method of Renshaw and Hotchkiss.[9] Trimethylamine, $N(CH_3)_3$, was bubbled into a solution of chloroacetamide, $ClCH_2CONH_2$ (10.1 g, 0.108 mol), in methanol (150 mL) for 15 min at room temperature. The solution was stirred for 1.5 h, after which the solvent was removed by rotary evaporation. The white crystalline product was recrystallized from ethanol, washed with ethyl ether and vacuum-dried (yield: 14.4 g, 87.9%). The ^1H NMR spectrum of a Me_2SO-d_6 solution gave resonances at −8.3, −7.7 ($-NH_2$); −4.2 ($-CH_2-$); and −3.2 ppm ($-CH_3$). In this and succeeding NMR data, the signs + and − denote resonances upfield and downfield, respectively, from tetramethylsilane.

Synthesis of $[(CH_3)_3NCH_2CONH_2]_2[Co(SC_6H_5)_4]\cdot{}^1/_2CH_3CN$ (1). Benzenethiol (0.92 g, 8.39 mmol) was dissolved in methanol (50 mL) under an inert atmosphere. Sodium (0.19 g, 8.39 mmol) was added to generate $NaSC_6H_5$. $CoCl_2$ (0.27 g, 2.1 mmol) and (CTA)Cl (0.64 g, 4.2 mmol) were added, and the green solution was stirred for 5 h. The solvent was evaporated under vacuum, leaving a green tar that foamed before hardening into a lacquer after 30 min. The product was maintained for 3 h under vacuum to further remove alcohol, following which it was dissolved in CH_3CN (40 mL). The solution was filtered to remove NaCl. The CH_3CN was removed by evaporation under vacuum, which was maintained while the resultant green tar was heated for 15 min at 55 °C. Ether (10 mL) was added under an inert atmosphere followed by CH_3CN (5 mL). The product transformed into a crystalline plaque within 15 min. Additional ether (20 mL) was introduced, and the product was dislodged with a spatula. The solvent was decanted and the product dried under vacuum (yield: 1.38 g, 90%). For X-ray crystallography, green well-formed crystals were obtained by the slow diffusion of ether vapor into a saturated CH_3CN solution of **1**. Elemental analysis was carried out by Galbraith Laboratories. Anal. Calcd for $C_{35}H_{47.5}N_{4.5}O_2S_4Co$: C, 56,02; H, 6.38; N, 8.40. Found: C, 55.97; H, 6.36; N, 8.07. The ^1H NMR spectrum of **1** was recorded in Me_2SO-d_6. Ligand peak assignments are −17.2, −16.70 (*m*-H); +24.4, +26.6 (*p*-H); and +33.2, +34.0 ppm (*o*-H) for the Co complex. Counterion proton signals appear at −8.2, −7.9 ($-NH_2$); −4.7 ($-CH_2-$); and −3.5 ppm ($-CH_3$).

Synthesis of $[(CH_3)_3NCH_2CONH_2][SC_6H_5]$ (2). Benzenethiol (0.487 g, 4.42 mmol) and sodium (0.102 g, 4.42 mmol) were reacted in ethanol (35 mL) to form $NaSC_6H_5$. (CTA)Cl (0.674 g, 4.05 mmol) was added as a solid, and the mixture was stirred for 60 min. The solution was filtered to remove NaCl. The filtrate was evaporated resulting in the formation of a thick paste. The product was redissolved in CH_3CN (40 mL) and the solution filtered to remove the remaining NaCl and $NaSC_6H_5$. The solvent was removed by evaporation under vacuum, and the product, a white precipitate, was washed three times with ethyl ether (30 mL) and vacuum-dried (yield: 0.72 g, 74%). Crystals for X-ray crystallography were obtained as colorless needles by the vapor diffusion of ether into a saturated CH_3CN solution. ^1H NMR (Me_2SO-d_6) resonances occur at −8.1, −7.7 ($-NH_2$); −7.0, −6.7, −6.4 ($-C_6H_5$); −4.1 ($-CH_2-$); and −3.2 ppm ($-CH_3$).

Methanol, acetonitrile, ether, and benzenethiol were distilled and stored under nitrogen before use. Chloroacetamide (Aldrich) was used as received.

Proton NMR data were acquired by using a General Electric QE 300 (300 MHz) spectrometer.

FTIR data were collected on a Nicolet 20F far-IR spectrometer on samples prepared as mineral oil mulls.

Samples for Raman experiments were prepared as mineral oil mulls and confined as a thin layer in the gap between coaxial NMR tubes for laser irradiation, inner tube 4-mm o.d. and outer tube 5-mm o.d. The Raman spectrometer consists of a SPEX 1401 double monochromator equipped with a SPEX 1914G photomultiplier tube and cooled housing. Laser radiation was provided by a Coherent 70-4 argon ion laser. An Anaheim Automation driver pack and stepper motor controlled the monochromator position and a CTO-386/20 computer controlled the driver pack and data collection. An EG&G Ortec ACE-MCS card and emulation software were used for the collection of photon counts and for data display. Data were processed by using "Spectra Calc" (Galactic Industries) software.

Table I. Crystallographic Data for $[(CH_3)_3NCH_2CONH_2]_2[Co(SC_6H_5)_4]\cdot{}^1/_2CH_3CN$ (**1**) and $[(CH_3)_3NCH_2CONH_2][SC_6H_5]$ (**2**)

	1	2
chem formula	$C_{35}H_{47.5}N_{4.5}O_2S_4Co$	$C_{11}H_{18}N_2OS$
fw	750.47	226.33
space group	$P\bar{1}$ (No. 2)	$P2_1/n$ (No. 14)
a, Å	16.960 (5)	12.847 (9)
b, Å	17.874 (6)	6.730 (5)
c, Å	14.184 (6)	29.268 (4)
α, deg	111.47 (3)	
β, deg	94.34 (3)	95.65 (2)
γ, deg	70.50 (2)	
V, Å	3767 (5)	2518 (2)
Z	2	8
T, °C	−70	23
λ, Å	0.710 69	1.541 78
ρ_{calcd}, g cm^{-3}	1.323	1.194
μ, cm^{-1}	7.02	20.61
trans coeff	0.85–1.11	0.66–1.55
R_1	0.048	0.048
R_2	0.051	0.060

X-ray Structure of $[(CH_3)_3NCH_2CONH_2]_2[Co(SC_6H_5)_4]\cdot{}^1/_2CH_3CN$ (1). X-ray data were collected on a Rigaku AFC-6S diffractometer equipped with a liquid-nitrogen low-temperature device (Table I). Details of data collection, reduction, and refinement procedures have been described elsewhere.[10] An absorption correction was applied by using the program DIFABS.[11] A total of 18 931 reflections ($+h,\pm k,\pm l$) were collected in the range $4° < 2\theta < 55°$. Of these 12 134 had $I_o > 2\sigma(I_o)$ and were used in the structure refinement, which was carried out by full-matrix least-squares techniques (838 variables) with the TEXSAN package of crystallographic programs from Molecular Structure Corp. Hydrogen atoms were placed in calculated positions except for those of the CH_3CN molecule of crystallization, which could not be located and were ignored. All non-hydrogen atoms were refined anisotropically. The final difference-Fourier map showed no significant features.

X-ray Structure of $[(CH_3)_3NCH_2CONH_2][SC_6H_5]$ (2). X-ray data were collected by using a Rigaku AFC-6S diffractometer (Table I). A total of 3684 reflections ($+h,+k,\pm l$) were collected in the range $4° < 2\theta < 110°$. The 2689 reflections with $I_o > 2\sigma(I_o)$ were used in the structure refinement, which was carried out by full-matrix least-squares techniques (272 variables) with the TEXSAN package.[10] An absorption correction was applied by using DIFABS.[11] Hydrogen atoms were placed in calculated positions and all non-hydrogen atoms were refined anisotropically. The final difference-Fourier map showed no significant features.

Results and Discussion

N–H···S Hydrogen Bonding. The asymmetric unit of **1** consists of two $[Co(SC_6H_5)]^{2-}$ anions and four $[(CH_3)_3NCH_2CONH_2]^+$ cations. The N–H···S bond lengths are unremarkable in **1**, with distances in the range 3.316 (3)–3.453 (3) Å (Table II). These values are within the range of N–H···S bond lengths observed in neutral organic compounds, 3.24–3.50 Å.[12] In the asymmetric unit the N–H···S hydrogen-bond distances are such that there is one long and one short length for each pair of hydrogen bonds associated with a Co(II) complex anion (Figure 1a and Table II). The central amide–amide dimer has short N–H···O hydrogen bonds of 2.965 (4) and 2.834 (4) Å, respectively (Figure 1a). Amide dimerization is a well-known structural motif.[13] The average N–H···O distance of 2.900 (4) Å is the same as the 2.901

(9) Renshaw, R. R.; Hotchkiss, H. T., Jr. *J. Am. Chem. Soc.* **1926**, *48*, 2698–2702.

(10) Young, A. C. M.; Walters, M. A.; Dewan, J. C. *Acta Crystallogr.* **1989**, *C45*, 1733–1736.

(11) Walker, N.; Stuart, D. *Acta Crystallogr.* **1983**, *A39*, 158–166.

(12) Hamilton, W. C.; Ibers, J. A. *Hydrogen Bonding in Solids*; Benjamin: New York, 1968; Chapter 5.

(13) Robin, M. B.; Bovey, F. A.; Basch, H. in *The Chemistry of the Amides*; Zabicky, J., Ed.; Wiley Interscience: New York, 1970.

Table II. Effects of Hydrogen Bonding on Selected Inter- and Intramolecular Distances (Å)

CTA-SC_6H_5-Co		CTA-SC_6H_5		acetamide[a]
		N-H···S		
S(2)-N(112)	3.317 (4)	S(1)-N(32)	3.290 (4)	
S(3)-N(122)	3.453 (3)	S(2)-N(42)[b]	3.271 (3)	
S(6)-N(92)	3.371 (4)	S(2)-N(42)	3.358 (3)	
S(6)-N(102)	3.316 (3)			
		$S-C_6H_5$ (Hydrogen Bonding)		
S(2)-C(21)	1.770 (4)	S(1)-C(11)	1.754 (3)	
S(3)-C(31)	1.761 (3)	S(2)-C(21)	1.757 (3)	
S(6)-C(61)	1.759 (3)			
		$S-C_6H_5$ (Non Hydrogen Bonding)		
S(1)-C(11)	1.759 (4)			
S(4)-C(41)	1.763 (4)			
S(5)-C(51)	1.772 (4)			
S(7)-C(71)	1.766 (4)			
S(8)-C(81)	1.769 (4)			
		C=O		
O(91)-C(95)	1.228 (5)	O(31)-C(35)	1.215 (4)	1.220 (3)
O(101)-C(105)	1.216 (4)[c]	O(41)-C(45)	1.235 (4)	
O(111)-C(115)	1.219 (4)			
O(121)-C(125)	1.236 (4)[c]			
		C-N		
N(92)-C(95)	1.324 (5)	N(32)-C(35)	1.313 (4)	1.380 (4)
N(102)-C(105)	1.327 (4)[c]	N(42)-C(45)	1.310 (4)	
N(112)-C(115)	1.329 (5)			
N(122)-C(125)	1.327 (4)[c]			

[a] Reference 33. [b] Atom is at $(^3/_2 - x, -^1/_2 + y, ^3/_2 - z)$. [c] Partner in amide dimer.

(2) Å observed in a neutron diffraction study[14] of crystalline acetamide. The amide dimer is slightly displaced toward the Co(2) complex anion (Figure 1 and Table II).

The hydrogen-bonding pattern differs for the two $[Co(SC_6H_5)_4]^{2-}$ anions of the asymmetric unit. In the Co(1) complex anion (Figure 1b), S(2) and S(3) are individually hydrogen bonded to amide N(112)-H(78) and N(122)-H(92), respectively. This type of amide-sulfur interaction is observed in the Tyr(11) N···Cys(9) S and Ala(44) N···Cys(42) S hydrogen-bonded pairs of oxidized Rd.[15-18] In the Co(2) complex anion (Figure 1c), S(6) is doubly hydrogen bonded to N(92)-H(52) and N(102)-H(65). Interactions of this type are observed in Rd as well, where Cys(6) S is hydrogen bonded to the amide N-H of both Val(8) N and Cys(9) N, and Cys(39) S is doubly hydrogen bonded to the amide N-H of Val(41) N and Cys(42) N.[15-18] As might be expected, the average hydrogen-bond length in the Co(II) complexes, 3.364 (4) Å (Table II), is shorter than that of oxidized Rd, 3.55 (12) Å,[15-18] where Cys is coordinated to Fe(III). The higher oxidation state of the protein metal ion reduces the hydrogen-bonding capacity of the coordinated thiolate ligands.

A comparison of the structure of the metal-free hydrogen-bonding adduct $[(CH_3)_3NCH_2CONH_2][S(C_6H_5)]$ (**2**) with that of the metal complex **1** shows the effects of the metal ion on the hydrogen-bond acceptor capacity of benzenethiolate. The hydrogen-bonding network of **2** has a central chain on a screw axis (Figure 2) with amide N(42) hydrogen bonded to benzenethiolate S(2). Amide N(42) is also hydrogen bonded to amide N(32) on the periphery of the central hydrogen-bonded spiral network. Last, benzenethiolate S(1) is hydrogen bonded to N(32). Single and double N-H···S hydrogen bonds are observed in **2** involving S(1) and S(2), respectively. Structural comparisons of **1**, **2**, and Rd[15-18] suggest that double N-H hydrogen bonding to thiolate sulfur may be relatively common. The average N-H···S distance in **2** is 3.306 (3) Å as compared with 3.364 (4) Å in **1**. The appreciably longer

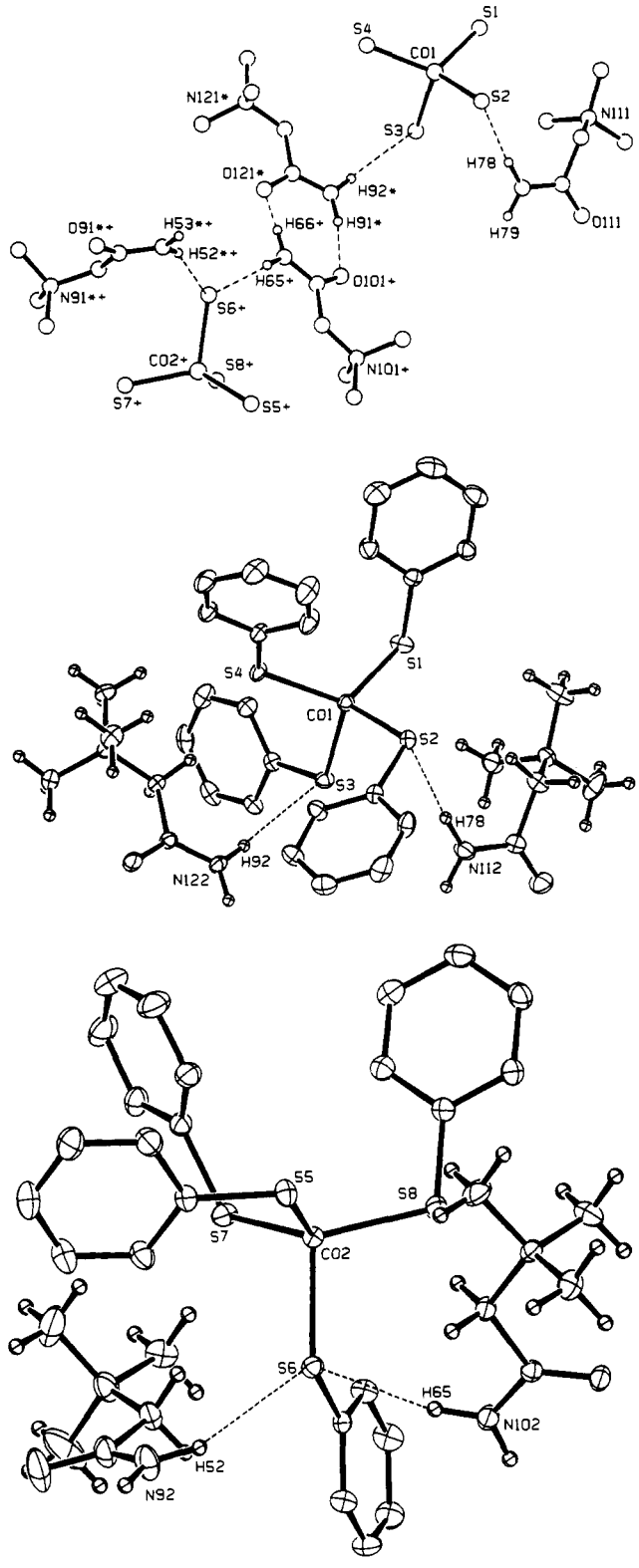

Figure 1. (a) Top: Diagram of the hydrogen-bonding network in $\{[(CH_3)_3NCH_2CONH_2]_2[Co(SC_6H_5)_4]\}_2$ (**1**). Atoms marked with an asterisk are at $(-x, -y, -z)$, those with a plus are at $(1 - x, -y, -z)$, and those with an asterisk and plus are at $(x, -1 + y, -1 + z)$. (b) Middle: ORTEP diagram of the CTA-Co(1) complex adduct of **1**. (c) Bottom: ORTEP diagram of the CTA-Co(2) complex adduct of **1**. For (b) and (c) the H-bonding interactions of the anionic complexes with the amide cations are shown along with atom-labeling schemes and 30% probability thermal ellipsoids.

(14) Jeffrey, G. A.; Ruble, J. R.; McMullan, R. K.; DeFrees, D. J.; Brinkley, J. S.; Pople, J. A. *Acta Crystallogr.* **1980**, *B36*, 2292-2299.
(15) Frey, M.; Sieker, L.; Payan, F.; Haser, R.; Bruschi, M.; Pepe, G.; LeGall, J. *J. Mol. Biol.* **1987**, *197*, 525-541.
(16) Watenpaugh, K. D.; Sieker, L. C.; Jensen, L. H. *J. Mol. Biol.* **1979**, *131*, 509-522.
(17) Watenpaugh, K. D.; Sieker, L. C.; Jensen, L. H. *J. Mol. Biol.* **1980**, *138*, 615-633.
(18) Adman, E. T.; Sieker, L. C.; Jensen, L. H.; Bruschi, M.; LeGall, J. *J. Mol. Biol.* **1977**, *112*, 113-120.

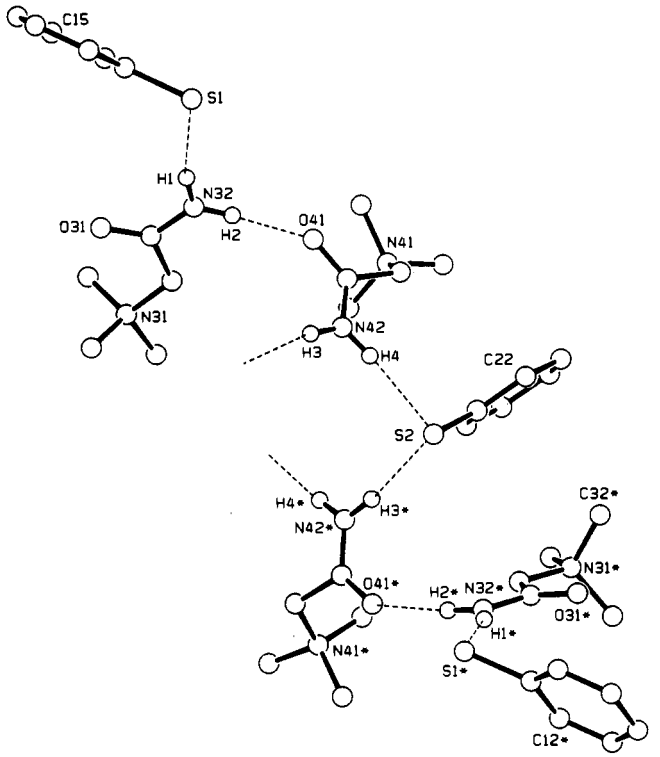

Figure 2. Diagram of the hydrogen-bonding network in the metal-free salt $[(CH_3)_3NCH_2CONH_2][SC_6H_5]$ (**2**). Atoms marked with an asterisk are at $(^3/_2 - x, -^1/_2 + y, ^3/_2 - z)$. H(3) is hydrogen bonded to S(2) (not shown), the latter being at $(^3/_2 - x, ^1/_2 + y, ^3/_2 - z)$. H(4*) is hydrogen bonded to S(2) (not shown), which is at $(^3/_2 - x, -^1/_2 + y, ^3/_2 - z)$.

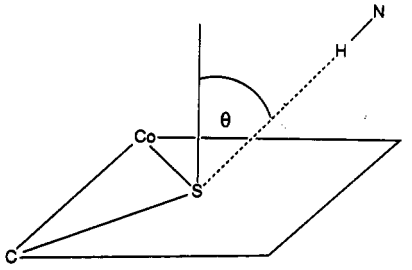

Figure 3. Schematic diagram of the Co–S–C plane. The dashed line represents the hydrogen bond linking N–H and S. θ is the angle formed by the hydrogen bond and the normal to the Co–S–C plane of the $[Co(SC_6H_5)_4]^{2-}$ anion.

N–H···S distance for metal-coordinated sulfur is evidence of the diminished capacity of the latter for hydrogen-bond formation.

In **1**, three of the N–H···S hydrogen bonds approach the normal to the plane containing the Co–S–C atoms of the metal–ligand complex (Figure 3). This is a standard geometry in systems where sulfur is in close proximity to electrophiles in a crystalline lattice.[19] It appears that an electrophile, in this case the N–H group, interacts preferentially with the sulfur lone pair that has substantial p-orbital character. The other lone pair can be considered to belong to an orbital with predominantly sp^2 character, which lies in the Co–S–C plane. As noted by Dunitz,[19] the most prevalent angle of electrophile approach is 20° relative to the normal to the Y–S–Z plane, where Y and Z are atoms covalently bonded to sulfur.

In the Co(1) complex anion, the hydrogen bonds N(112)–H(78)···S(2) and N(122)–H(92)···S(3) deviate by 8.45 and 24.66° from the normals to their respective Co–S–C planes. The angle formed by the N(122)–H(92)···S(3) bond with the normal occurs within the expected range. However, the N(112)–H(78)···S(2) bond forms a very small angle with the normal. The corresponding Co–S(2) bond is much shorter than expected, the significance of which is discussed below.

In the Co(2) complex anion, where S(6) is hydrogen bonded to both N(92)–H(52) and N(102)–H(65), the interaction involves both sulfur lone-pair orbitals. Hydrogen bonds to S(6) are 3.371 (4) and 3.316 (3) Å in length, respectively. They sit on either side of the Co–S–C plane and deviate by 38.2 and 20.2°, respectively, from the perpendicular axis passing through the plane. The angle between the hydrogen bonds, H(52)···S(6)···H(65), is 123.2°. These results suggest a sulfur valence orbital hybridization that is intermediate between sp^3 and sp^2 + p.

The ionic hydrogen bond, as described by Morokuma and co-workers using energy decomposition, is maintained principally by electrostatic and charge-transfer interactions.[20] The presence of N–H···S hydrogen bonds affects bond lengths between cobalt and sulfur in **1** and within the amide groups of both **1** and **2**.

Co–S Bonds. The average Co–S bond length in **1**, involving non-hydrogen-bonded sulfur (S_N), is 2.294 (2) Å, shorter by 0.034 Å than the average Co–S bond length in $[(C_6H_5)_4P]_2[Co(SC_6H_5)_4]$ of 2.328 (4) Å (Table III). The latter complex, whose structure was reported by Coucouvanis and co-workers,[21] is devoid of hydrogen-bonding interactions. The decrease in Co–S_N bond lengths in **1** indicates a strengthening of these metal–ligand bonds by amide–thiolate N–H···S_H hydrogen bonding. This change likely results from the withdrawal of electron density from the S_H (hydrogen-bonded sulfur) ligands into the amide framework, as expected for hydrogen-bonded adducts.[22] The Co–S_H bonds have an average length in **1** of 2.320 (2) Å, essentially unchanged from that of the Co–S bonds in the non-hydrogen-bonding complex $[(C_6H_5)_4P]_2[Co(SC_6H_5)_4]$.

From the point of view of molecular orbitals, thiolate sulfur is a σ- and π-electron donor. The π orbitals, occupied by lone-pair electrons,[23] interact with occupied p and d orbitals on the metal.

Table III. Selected Bond Distances (Å) and Angles (deg) for $[Co(SC_6H_5)_4]^{2-}$ Complex Anions

Selected Atomic Distances

$[(CH_3)_3NCH_2CONH_2]_2[Co(SC_6H_5)_4]$[a]			
Co(1)–S(1)	2.299 (2)	Co(2)–S(5)	2.294 (1)
Co(1)–S(2)[c]	2.299 (1)	Co(2)–S(6)[c]	2.328 (1)
Co(1)–S(3)[c]	2.321 (1)	Co(2)–S(7)	2.276 (11)
Co(1)–S(4)	2.295 (1)	Co(2)–S(8)	2.305 (1)
$[(C_6H_5)_4P]_2[Co(SC_6H_5)_4]$[b]			
Co–S(1)	2.326 (4)	Co–S(3)	2.316 (4)
Co–S(2)	2.342 (4)	Co–S(4)	2.328 (4)

Selected Bond Angles

$[(CH_3)_3NCH_2CONH_2]_2[Co(SC_6H_5)_4]$[a]			
S(1)–Co(1)–S(2)[c]	105.21 (5)	Co(1)–S(1)–C(11)	110.2 (1)
S(1)–Co(1)–S(3)[c]	103.73 (5)	Co(1)–S(2)[c]–C(21)	111.0 (1)
S(1)–Co(1)–S(4)	119.64 (5)	Co(1)–S(3)[c]–C(31)	112.7 (1)
S(2)[c]–Co(1)–S(3)[c]	106.26 (4)	Co(1)–S(4)–C(41)	115.6 (1)
S(2)[c]–Co(1)–S(4)	116.07 (5)	Co(2)–S(5)–C(51)	107.5 (1)
S(3)[c]–Co(1)–S(4)	104.51 (4)	Co(2)–S(6)[c]–C(61)	116.3 (1)
S(5)–Co(2)–S(6)[c]	102.07 (4)	Co(2)–S(7)–C(71)	115.9 (1)
S(5)–Co(2)–S(7)	115.91 (5)	Co(2)–S(8)–C(81)	110.6 (1)
S(5)–Co(2)–S(8)	110.76 (4)	N(92)–H(52)···S(6)	160.9 (2)
S(6)[c]–Co(2)–S(7)	105.55 (5)	N(102)–H(65)···S(6)	162.1 (2)
S(6)[c]–Co(2)–S(8)	105.61 (5)	N(112)–H(78)···S(2)	171.3 (2)
S(7)–Co(2)–S(8)	115.32 (5)	N(122)–H(92)···S(3)	159.5 (2)
$[(C_6H_5)_4P]_2[Co(SC_6H_5)_4]$[b]			
S(1)–Co–S(2)	95.6 (2)	S(1)–Co–S(4)	114.8 (2)
S(3)–Co–S(4)	97.0 (2)	S(2)–Co–S(3)	113.5 (2)
S(1)–Co–S(3)	121.3 (2)	Co–S–C(av)	109.9 (2.2)
S(2)–Co–S(4)	116.1 (2)		

[a] This work. [b] Reference 21. [c] Hydrogen bonding.

(19) Rosenfield, R. E., Jr.; Parthasarathy, R.; Dunitz, J. D. *J. Am. Chem. Soc.* **1977**, *99*, 4860–4862.

(20) Umeyama, H.; Morokuma, K. *J. Am. Chem. Soc.* **1977**, *99*, 1316–1333.

(21) Swenson, D.; Baenziger, N. C.; Coucouvanis, D. *J. Am. Chem. Soc.* **1978**, *100*, 1933–1934.

(22) Sheridan, R. P.; Allen, L. C. *Chem. Phys. Lett.* **1980**, *69*, 600–604.

These metal orbitals have antibonding character, and their occupation results in a weakening of the M–S interaction.[24] It is expected that hydrogen bonding stabilizes the sulfur π-donor orbitals and thereby diminishes the Co–S antibonding interaction. This should result in a shortening of *both* the Co–S_N and the Co–S_H bonds, which surprisingly is not observed in the latter. On the other hand, the hydrogen bond may impart partial thioether character to the S_H ligand, which would then impose a weaker ligand field than non-hydrogen-bonded thiolate S_N.[25] However, the sulfur lone-pair electrons are conjugated with the phenyl ring π electrons,[26] which might explain why the Co–S_H bonds in **1** are not longer on average than metal ligand bonds in the $[(C_6H_5)_4P]_2[Co(SC_6H_5)_4]$ complex.

This leaves the short Co–S_H(2) bond length to explain. It has been observed with oxygen and nitrogen lone-pair donors that the extent of electron donation to a hydrogen-bonding acceptor increases with p-orbital character of the lone-pair orbital.[27] As discussed above, the Co(1)–S_H(2) bond of 2.299 Å is shorter than expected in comparison with the lengths of the Co(1)–S_H(3) bond of 2.321 Å and Co(2)–S_H(6) of 2.328 Å. This might be related to the observation, discussed above, that the deviation of the N–H···S(2) vector from the normal to the Co–S–C plane is particularly small. It is also observed that the N(112)–H(78)···S(2) bond more closely approaches linearity than do the other three (Table III). Thus, a possible explanation for the short Co–S_H(2) bond length is that the hydrogen bond utilizes an orbital on S_H(2) with nearly pure p character, orthogonal to, and therefore having little influence on, the Co–S_H σ orbital.

As observed in a recent study of hydrogen bonding between dialkylammonium ions and $[Co(SC_6H_5)_4]^{2-}$ complex anions,[28] shortening of the metal–thiolate bond lengths results from the ammonium–thiolate N–H···S hydrogen-bond formation. It appears that the amide–thiolate N–H···S interaction similarly provides an *overall* stabilizing influence in **1**, whose average Co–$S_{(H+N)}$ bond length is 2.302 (2) Å, which is 0.026 Å shorter than the average of the corresponding bonds in $[(C_6H_5)_4P]_2[Co(SC_6H_5)_4]$ of 2.328 Å.

The Co–S bond angles likewise manifest the effects of hydrogen bonding. There is a marked change in S–Co–S bond angles as a function of S_N or S_H character. The average S_N–Co–S_N bond angle, 115.41 (5)°, is significantly larger than either S_H–Co–S_N or S_H–Co–S_H bond angles (Table III), which have average values of 106.11 (5) and 106.26 (4)°, respectively. The angle for S(2)–Co(1)–S(4), 116.07 (5)°, is anomalously large in conjunction with the particularly short Co–S(2) length. In the non-hydrogen-bonding complex $[(C_6H_5)_4P]_2[Co(SC_6H_5)_4]$, the elongated D_{2d} structure has two S–Co–S angles of average value 96.3° and four S–Co–S angles of average value 116.4°.[21]

Bis(*o*-xylene-α,α'-dithiolato)ferrate(II,III) anions have been employed as structural models for the tetrakis(cysteinato)iron(II,III) site of Rd.[5,6] The average Fe–S bond lengths of the reduced and oxidized anions are 2.356 (13) and 2.267 (3) Å, respectively, a difference of 0.089 Å. By comparison, the average decrease in the Co–S_N bond lengths is 38% of that value, 0.034 Å. The Co–S_N bonds are strengthened by hydrogen bonds just as they would be if the metal were to undergo an oxidation. What is more striking is that the Co–S_N bond length decrease in **1** represents approximately 56% of the average Fe–S bond length difference of 0.061 Å for reduced and oxidized Rd as determined by EXAFS.[29] For Rd, in which *all* of the cysteine thiolate sulfur atoms are hydrogen bonded to peptide amide groups, the degree of stabilization of the metal center as reflected in the protein redox potential is probably greater. It is important to consider however that since thiolate S_N is absent in Rd, hydrogen bonding may not result in relatively short Fe–S_{Cys} bonds.

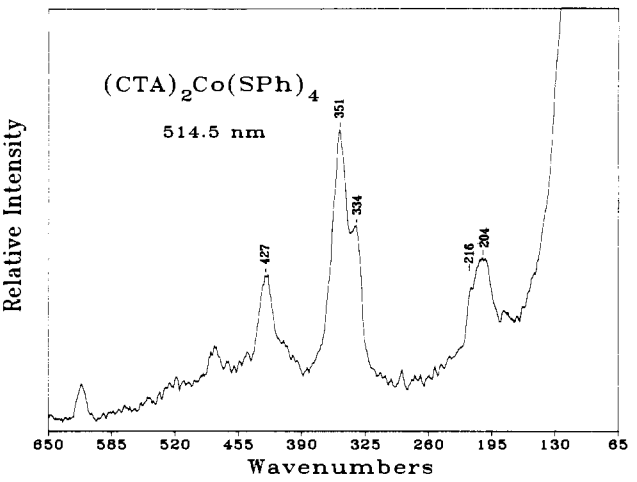

Figure 4. Raman spectrum of **1** [CTA = (carbamoylmethyl)trimethylammonium, SPh = SC_6H_5]. Data were collected in 150° backscattering geometry. The excitation wavelength was 514.5 nm, 20 mW, and the spectral band pass, 10 cm^{-1}. The monochromator was advanced in 1-cm^{-1} increments with a data collection time of 1 s/point. Data were processed by a 7 point Savitsky–Golay smoothing routine.

Amide Bond Lengths. In concert with metal–ligand bond length changes it is expected that the N–H and C=O bonds in CTA would be lengthened by the hydrogen-bond interaction, while the C–N bond would be shortened.[30-33] In this work however N–H bond lengths could not be determined, and no difference was discerned between the C=O bonds of **1** and **2** (Table II). By contrast, a clear trend of decreasing C–N bond length is evident in comparing electron diffraction data on non-hydrogen-bonding acetamide in the gas phase[33] with X-ray diffraction data on the acetamide moiety hydrogen bonded to thiolate ion that is free in **2** and ligated to Co in **1** (Figures 1 and 2 and Table II). The C–N bond length varies from 1.380 (4) Å in the gas phase[33] to 1.313 (4) Å in the solid-state amide–thiolate pair. This is the manifestation of electron density shifts in the amide, H→N, N→C, and C→O, that occur upon hydrogen-bond formation.[22,30,31] The C–N bond length for crystalline acetamide, 1.337 Å,[14] results from N–H···O hydrogen bonding and is equivalent to the distance observed for amide hydrogen bonded to thiolate in **1**.

The effect of hydrogen bonding on the C–N bond lengths is related to the effect observed in other Lewis acid–base donor–acceptor pairs. In the trichlorophosphite–pentachloroantimony system, $Cl_3P{=}O{\rightarrow}SbCl_5$, for example,[34] the P=O bond is lengthened and the Cl–P bonds are shortened relative to bonds in free $POCl_3$. As pointed out by Gutman and co-workers,[30,31] these shifts are expected as a consequence of electron density shifts to the less electronegative atom of a bonded pair. Amide bond lengths could in principle provide an indication of the degree of stabilization provided by hydrogen bonding in reduced Rd.

Vibrational Spectroscopy. The Raman spectrum of **1** (Figure 4) is quite similar in most respects to that of the non-hydrogen-bonding complex $[(CH_3)_4N]_2[Co(SC_6H_5)_4]$. In previous work[28] we have assigned a Raman band at 201 cm^{-1} in the latter complex to a Co–S vibrational mode. In **1** the analogous band appears at 204 cm^{-1}, consistent with a slight increase in the metal–ligand

(23) Kamata, M.; Hirotsu, K.; Higuchi, T.; Kido, M.; Tatsumi, K.; Yoshida, T.; Otsuka, S. *Inorg. Chem.* **1983**, *22*, 2416–2424.
(24) Harris, S. *Polyhedron* **1989**, *8*, 2843–2882.
(25) Kuehn, C. G.; Isied, S. S. In *Progress in Inorganic Chemistry*; Lippard, S. J., Ed.; Wiley: New York, 1980; Vol. 27, pp 153–212.
(26) March, J. *Advanced Organic Chemistry*; Wiley: New York, 1985; Chapter 9.
(27) Sherry, A. D. In *The Hydrogen Bond*; Schuster, P., Zundel, G., Sandorfy, C., Eds.; North Holland Publishing Co.: New York, 1976.
(28) Chung, W. P.; Dewan, J. C.; Walters, M. A. *J. Am. Chem. Soc.* **1991**, *113*, 525–530.
(29) Shulman, R. G.; Eisenberger, P.; Teo, B.; Kincaid, B. M.; Brown, G. S. *J. Mol. Biol.* **1978**, *124*, 305–331.
(30) Gutman, V.; Resch, G.; Linert, W. *Coord. Chem. Rev.* **1982**, *43*, 133–164.
(31) Gutman, V. *The Donor-Acceptor Approach to Molecular Interactions*; Plenum: New York, 1978; Chapter 1.
(32) Gutman, V. *Electrochim. Acta* **1976**, *21*, 661–670.
(33) Kitano, M.; Kuchitsu, K. *Bull. Chem. Soc. Jpn.* **1973**, *46*, 3048–3051.
(34) (a) Lindqvist, I. *Inorganic Adduct Molecules of Oxo-Compounds*; Springer-Verlag: Berlin, 1963; pp 65–69. (b) Lindqvist, I.; Branden, C.-I. *Acta Crystallogr.* **1959**, *12*, 642–645.

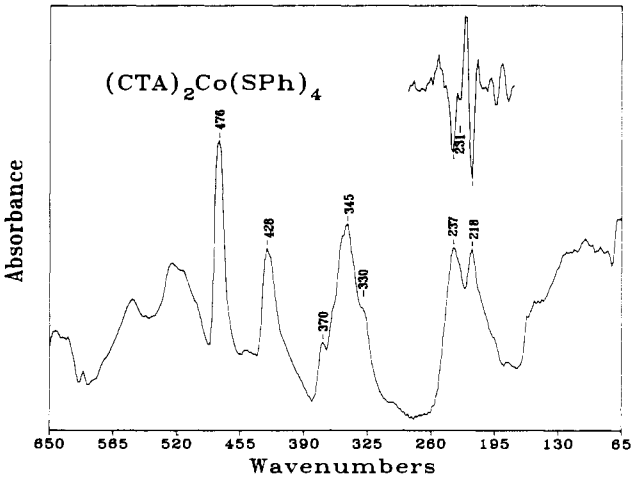

Figure 5. FTIR spectrum of **1** [CTA = (carbamoylmethyl)trimethylammonium, SPh = SC_6H_5]. The truncated spectrum (top) is a second derivative of the corresponding frequency region in the lower spectrum. The data represent an average of 600 scans obtained at 4-cm^{-1} resolution. For the second derivative a 5 point Savitzky–Golay smoothing routine was carried out on the absorption data followed by a 7 point polynomial fit for calculation of the derivative.

force constants that accompany a decrease in bond length. This band is likely derived from an A_1 (symmetric) stretching mode that would occur in a complex with ideal T_d symmetry. The shoulder at 216 cm^{-1} correlates roughly with the band at 218 cm^{-1} in the IR spectrum. It too may be assigned to a Co–S stretch.

Metal–ligand asymmetric stretching modes likely occur in the 230-cm^{-1} region as observed in the infrared spectrum of $[(CH_3)_4N]_2[Co(SC_6H_5)_4]$.[28] The infrared spectrum of **1** (Figure 5) shows a broad feature in that region with two maxima at 237 and 219 cm^{-1}. The 237-cm^{-1} band has a shoulder at 231 cm^{-1}, as determined by a second-derivative calculation. These three bands are shifted relative to analogous bands in $[(CH_3)_4N]_2[Co(SC_6H_5)_4]$[28] observed at 235, 228, and 220 cm^{-1}. The latter are assigned to metal–ligand modes related to the T_2 (asymmetric) stretching modes of a complex with ideal T_d symmetry. The frequency distribution in **1** reflects the low symmetry of the complexes in the crystal structure, which causes the degenerate T_2 mode to split into a triplet. The bands at 237 and 231 cm^{-1} are shifted up in frequency relative to those in the non-hydrogen-bonding complex, probably as a result of Co–S_N bond shortening induced by hydrogen bonding. The band at 218 cm^{-1} may be correlated with the longer Co–S_H bonds that are directly hydrogen bonded to amide. From use of a Badger's rule approximation,[35] an upper limit frequency increase of 15 cm^{-1} is expected for a bond length decrease of 0.054 Å, the bond length difference between Co(2)–S(6) and Co(2)–S(7).

An overall broadening is observed for the T_2 asymmetric stretching mode of **1** relative to the complex $[(CH_3)_4N]_2[Co(SC_6H_5)_4]$. A similar apparent broadening is seen in the 204-cm^{-1} band. Band broadening in these two cases could be due to the lower symmetry of the hydrogen-bonding complex anions relative to the non-hydrogen-bonding control complex. The Co(1) and Co(2) complex anions have approximate C_{2v} and C_{3v} local symmetry, respectively. The symmetry of $[(CH_3)_4N]_2[Co(SC_6H_5)_4]$ is inferred from the crystallographic data on the non-hydrogen-bonding complex $[(C_6H_5)_4P]_2[Co(SC_6H_5)]$, which has D_{2d} symmetry.[21,36]

Just as with other bonds in **1** and **2**, S_H–C bonds should be sensitive to hydrogen bonding. In fact, they are found to be 0.01 Å shorter on average than S_N–Co bonds (Table II). Although this difference is small considering the magnitude of the uncertainty, it should be reflected in changes in S–C force constants. However, the S–C vibration of benzenethiolate is strongly coupled to phenyl ring modes[37] and the effect of hydrogen bonding is delocalized and difficult to measure spectroscopically.

Electronic Absorption Spectra. The visible spectrum of **1** was recorded with the sample dispersed in a KBr pellet. Bands corresponding to the $A_2 \rightarrow {}^4T_1(P)$ transition of Co(II) were observed at 747 (13 386) and 693 nm (14 430 cm^{-1}), with a shoulder at 640 nm (15 625 cm^{-1}). These bands are assigned on the basis of a comparison with the spectral assignments of the $[Co(SC_6H_5)_4]^{2-}$ anion in solution.[21,38] The solid-state visible spectrum of the non-hydrogen-bonding complex $[(CH_3)_4N]_2[Co(SC_6H_5)_4]$ revealed bands at 746 (13 405), 692 (14 451), and 654 nm (15 291 cm^{-1}).[28] Amide–thiolate hydrogen bonding has virtually no effect on the ligand field spectrum of the $[Co(SC_6H_5)_4]^{2-}$ anion. A band is observed at 424 nm, which corresponds to the charge-transfer band at 420 nm in the spectrum of $[(CH_3)_4N]_2[Co(SC_6H_5)_4]$[28] and is likewise negligibly affected by hydrogen bonding.

The ligand field electronic transitions of tetrahedral Co(II) are altered by hydrogen bonding, which is expected to split the ${}^4T_2(F)$, ${}^4T_1(F)$, and ${}^4T_1(P)$ states as the microsymmetry of the anion is transformed from effective D_{2d}[21] to C_{3v} for the Co(2) complex anion and D_{2d} to C_{2v} for the Co(1) complex anion. However, because of the simultaneous lengthening and shortening of Co–S bonds, the change in the average ligand field is slight. As a result, the d–d bands in the vicinity of 650 nm are broadened but unshifted relative to those of $[(CH_3)N]_2[Co(SC_6H_5)_4]$.

Energetics. Amide–thiolate dimerization energies have been predicted to occur in the vicinity of 20 kcal mol^{-1}.[39] In recent work, Sellman[40] has estimated that hydrogen bonding between diazene and thiolate sulfur ligands in an iron–sulfur complex accounts for a 17 kcal mol^{-1} stabilization of the diazene ligand. In **2** it is reasonable to consider that the amide might be stabilized to a similar extent. In **1** amide stabilization should be less due to the loss of sulfur electron density to Co–S bonds. The stabilization of Co–S_N bond energies in **1** can be estimated from the 3-cm^{-1} vibrational frequency shift in the A_1 mode as a result of hydrogen bonding. This determination is based on two assumptions: (1) The ratio of force constants for a specific normal mode in a series of closely related isomorphous molecules is proportional to the spectroscopic dissociation energies of the molecules. (2) The spectroscopic dissociation energy, D_e, for the Co(II)–SR bond is assumed to be close to that for the Fe(II)–SR bond, which is approximated by the average of D_e for FeF_2 and $FeCl_2$; $D_e(FeF_2) > D_e(FeSR) \approx D_e(CoSR) > D_e(FeCl_2)$. The basis for assumption 1 is empirical. For a series of related molecules the force constant, which is an expression of the curvature of the bottom of the well of a parabolic potential function, is generally observed to increase linearly with bond dissociation enthalpy.[41] Assumption 2 is a chemically reasonable approach given that (a) RS^- falls between F^- and Cl^- in the spectrochemical series[42] and (b) the free energies of hydration and ligation for Fe^{2+} and Co^{2+} are similar.[43] The molar bond dissociation energy ΔH_m is related to the bond dissociation energy by the expressions[44]

$$\Delta H_m = D_o(\text{molar}) + RT \quad (1a)$$

$$D_e = D_o + \tfrac{1}{2}[1 - \tfrac{1}{2}\chi_e]h\nu \quad (1b)$$

where D_e and D_o are the spectroscopic and chemical bond dissociation energies, χ_e is the anharmonicity constant, and $^1/_2h\nu$ is the zero-point energy for the A_1 mode, which is taken to be

(35) Herschbach, D. R.; Laurie, V. W. *J. Chem. Phys.* **1961**, *35*, 458–463.
(36) Swenson, D. C. Ph.D. Thesis, University of Iowa, May 1979.
(37) Dollish, F. R.; Fateley, W. G.; Bentley, F. F. *Characteristic Raman Frequencies of Organic Compounds*; Wiley: New York, 1974; Chapter 5.
(38) Dance, I. G. *J. Am. Chem. Soc.* **1979**, *101*, 6264–6273.
(39) Sheridan, R. P.; Allen, L. C.; Carter, C. W. *J. Biol. Chem.* **1981**, *256*, 5052–5057.
(40) Sellman, D.; Soglowek, W.; Knoch, F. *Angew. Chem., Int. Ed. Engl.* **1989**, *28*, 1271–1272.
(41) Nakamoto, K. *Infrared and Raman Spectra of Inorganic and Coordination Compounds*; John Wiley and Sons: New York, 1986; pp 11–12.
(42) Jorgensen, C. K. *Inorg. Chim. Acta Rev.* **1968**, *2*, 65–88.
(43) Figgis, B. N. *Introduction to Ligand Fields*; John Wiley and Sons: New York, 1966; p 91.
(44) Atkins, P. W. *Physical Chemistry*; W. H. Freeman and Co.: New York, 1986; pp 450–452.

approximately 0.6 kJ mol^{-1} (100 cm^{-1}) for both hydrogen-bonded and control complexes. We make the approximation $\Delta H_m \approx D_e$, since RT and the second term of eq 1b are small. Then, from the chemical dissociation energies for Fe compounds[45]

$$D_e(Co^{2+}\text{-}SR) \approx D_e(Fe^{2+}\text{-}SR) \approx \tfrac{1}{2}[D_o(Fe^{2+}\text{-}F) + D_o(Fe^{2+}\text{-}Cl)] = \tfrac{1}{2}[481 \text{ kJ mol}^{-1} + 400 \text{ kJ mol}^{-1}] = 440.5 \text{ kJ mol}^{-1} \quad (2)$$

The approximate stabilization energy is then determined from the frequency shift of the "A_1" mode on the basis of the approximate relationship

$$\begin{aligned}\Delta D_e &= D_e(Co^{2+}\text{-}SR)\{[K(A_1,\text{H-bonding})/K(A_1,\text{control})] - 1\} \\ &= D_e(Co^{2+}\text{-}SR)\{[\nu(A_1,\text{H-bonding})/\nu(A_1,\text{control})]^2 - 1\} \\ &= 440.5 \text{ kJ mol}^{-1}\{[204 \text{ cm}^{-1}/201 \text{ cm}^{-1}]^2 - 1\} \\ &= 13.2 \text{ kJ mol}^{-1} (3.16 \text{ kcal mol}^{-1}) \quad (3)\end{aligned}$$

where K is the force constant for $\nu(A_1)$.

The stabilization effect of N-H···S hydrogen bonding on metal-sulfur bonds is expected to be similar for Co and Fe complexes and could plausibly occur in iron-sulfur centers in Fe-S proteins. Such an effect could account for the higher reduction potentials found for Fe-S proteins as compared with their non-hydrogen-bonding synthetic active-site analogues. This would require that the differential stabilization of the redox center in its reduced state be greater than that of the oxidized state,[22] an effect that has been substantiated in the study of metal complexes in hydrogen-bonding liquids.[46]

Conclusion. Structural data give clear evidence for the stabilization of metal-thiolate bonds in the hydrogen-bonded complex **1**. The average Co-S_N and Co-$S_{(H+N)}$ bond lengths are shortened 0.034 and 0.026 Å, respectively, relative to those in the non-hydrogen-bonded complex $[(C_6H_5)_4P]_2[Co(SC_6H_5)_4]$.[21] This should be compared to the average bond length change of 0.089 Å in the bis(*o*-xylene-α,α'-dithiolato)ferrate(II,III) complex anions[6] and 0.061 Å in Rd,[29] which accompanies a one-electron oxidation-state change in iron. The amide C-N bond is substantially stabilized by hydrogen bonding,[14] as evidenced by its marked decrease in length in **1** and **2** relative to the gas phase (Table II).[33,47] Vibrational frequencies of normal modes related to $T_2(T_d)$ and $A_1(T_d)$ metal-ligand modes increase, consistent with a stabilization of certain of the metal-ligand bonds via hydrogen bonding.

The experiments described here focus on a single oxidation state of a complex where the central metal is in the 2+ state. It is expected, however, on the basis of theoretical work, that hydrogen-bond stabilization will be less for a complex with a metal in the 3+ state.[22] If structural studies bear this out, then an argument can be made for a substantial role for hydrogen bonding in the modulation of redox potentials in iron-sulfur proteins.

Acknowledgment. We thank Professors L. C. Allen, C. Deakyne, O. Knop, and K. Theopold and Dr. W. L. Duax for helpful discussions.

Supplementary Material Available: General structure reports for compounds **1** and **2** including details of the structure determination, listings of experimental details, positional and thermal parameters, inter- and intramolecular bond distances and bond angles involving non-hydrogen atoms, and intermolecular distances involving hydrogen atoms, and PLUTO diagrams of the structures (98 pages); a listing of final observed and calculated structure factors (101 pages). Ordering information is given on any current masthead page.

(45) (a) Huheey, J. E. *Inorganic Chemistry*; Harper and Row: New York, 1983, pp A-28-A-40. (b) Feber, R. C. Los Alamos Report LA-3164, 1965.

(46) Gutmann, V. In *Structure and Bonding*; Springer-Verlag: New York, 1973; Vol. 15, pp 141-166.

(47) Popelier, P.; Lenstra, A. T. H.; Van Alsenoy, C.; Geise, H. J. *J. Am. Chem. Soc.* **1989**, *111*, 5658-5660.

Contribution from the Department of Chemistry, Massachusetts Institute of Technology, Cambridge, Massachusetts 02139, and Department of Radiology, Harvard Medical School and Brigham and Women's Hospital, Boston, Massachusetts 02115

Technetium(III) Complexes with the Tetradentate "Umbrella" Ligand Tris(*o*-mercaptophenyl)phosphinate: X-ray Structural Characterization of $Tc(P(o\text{-}C_6H_4S)_3)(CNC_3H_7)$ and $Tc(P(o\text{-}C_6H_4S)_3)(CNC_3H_7)_2$

Nadine de Vries,[1a] Jessica Cook,[1a] Alun G. Jones,[1b] and Alan Davison*[,1a]

Received November 27, 1990

Tris(*o*-mercaptophenyl)phosphinate (PS3) binds to Tc(III) as a tetradentate ligand to form the formally 14-electron complex Tc(PS3)(CNMe). An X-ray single-crystal structure determination of the isopropyl isocyanide derivative Tc(PS3)(CN-*i*-Pr) shows that the complex has a trigonal-bipyramidal geometry with the phosphorus and isonitrile carbon in the axial positions and the sulfurs bound in the equatorial plane (crystal data: MF = $C_{22}H_{19}NPS_3Tc$, monoclinic, a = 10.3541 (8) Å, b = 13.2274 (6) Å, c = 16.437 (1) Å, β = 90.855 (6)°, space group $P2_1/c$, Z = 4; final R = 0.049, R_w = 0.057). In the presence of a large excess of isonitrile, these electron-deficient complexes bind a sixth ligand. The six-coordinate complex Tc(PS3)(CN-*i*-Pr)$_2$, was also structurally characterized (crystal data: MF = $C_{26}H_{26}N_2PS_3Tc$, orthorhombic, a = 18.896 (1) Å, b = 13.2815 (8) Å, c = 10.3823 (6) Å, space group $Pna2_1$, Z = 4; final R = 0.044, R_w = 0.048).

Introduction

The ligand 2,3,5,6-tetramethylbenzenethiolate (tmbt) has been shown to stabilize technetium in the +3 oxidation state.[2] Compounds such as $Tc(tmbt)_3(MeCN)_2$ exhibit trigonal-bipyramidal geometry with three thiols in the equatorial plane and two π-accepting ligands in the axial positions. The acetonitrile ligands are labile and undergo substitution through a proposed six-coordinate intermediate, allowing the incorporation of any number of π-accepting ligands, CN-*i*-Pr, py, CO, MeCN, or PEt_3, into the axial positions.

We have now designed a chelating "umbrella" ligand, tris(*o*-mercaptophenyl)phosphinate (PS3), which provides technetium with three thiolate ligands and one of the axial π-accepting ligands while leaving the fifth coordination site open for ligand exchange. With this umbrella system, the six-coordinate complex can be isolated, indicating that this is the intermediate involved in the ligand-exchange reactions of the trithiolate compounds described above.

Experimental Section

Caution! Technetium-99 is a weak β-emitter (E = 0.292 MeV, $t_{1/2}$ = 2.12 × 10^5 years). All work has been done in laboratories approved

(1) (a) Massachusetts Institute of Technology. (b) Harvard Medical School.

(2) de Vries, N.; Dewan, J. C.; Jones, A. G.; Davison, A. *Inorg. Chem.* **1988**, *27*, 1574.

0020-1669/91/1330-2662$02.50/0